J Mater Sci (2009) 44:4354–4359
DOI 10.1007/s10853-009-3650-1

Phase transition characteristics and electrical properties of nitrogen-doped GeSb thin films for PRAM applications

Seung Yun Lee · Hyung Keun Kim · Jin Hyock Kim · Jae Sung Roh · Doo Jin Choi

Received: 12 January 2009 / Accepted: 28 May 2009 / Published online: 14 June 2009

Abstract We have investigated the nitrogen doping effect on phase transition characteristics and electrical property of nitrogen-doped GeSb (N-doped GS) thin films. The nitrogen gas flow rate changed from 0 sccm (GS(0)) to 6 sccm (GS(6)) during the deposition. The sheet resistance of crystalline state was increased from 2.6 to 5.1 kΩ/□ and thermal stability of amorphous was increased as nitrogen gas flow rate increased due to nitrogen doping effect. Moreover, the average grain size was decreased from 9.7 to 6.6 nm at 400 °C as nitrogen gas flow rate increased. However, the crystallization threshold time and laser power of GS(6) were shorter and lower than GS(0) caused by lower optical reflectivity. Nitrogen-doped GeSb showed the possibility of low RESET power and high speed PRAM operation.

Introduction

Phase-change random access memory (PRAM) is one of the most optimized candidates for the next generation non-volatile memory due to its fast operation speed, high scalability, low power operation, and fabrication costs [1]. Among phase change materials (PCM), Sb-rich GeSb was interested for phase change optical record taking advantages of its ultrafast crystallization speed and high optical reflectivity difference. In Sb-rich GeSb, Sb shows rapid crystallization characteristics due to its grain growth dominated crystallization nature and high optical reflectivity difference, while Ge helps stability of amorphous phase [2]. Recently, doped GeSb was researched for the solid state memory applications using its large difference in electrical resistance and a fast phase transition speed between amorphous and crystalline phase. The GeSb has some advantages for PRAM applications comparing with $Ge_2Sb_2Te_5$ such as a higher crystallization temperature, fast crystallization speed, and binary composition [3]. The high crystallization temperature prevents loosing data during set and reset operations and the fast crystallization speed increases especially the total operation speed of PRAM because the set operation is the slowest operation. In addition, since GeSb is binary composition, deposition process is easier than the ternary composition. However, in order to be prime candidate for the next PCM, GeSb needs to improve some drawbacks. The crystalline resistance of GeSb is higher than $Ge_2Sb_2Te_5$ but still not enough for the future PRAM applications. Therefore, we doped nitrogen in GeSb thin film by DC magnetron reactive sputtering system since nitrogen is well-known for increasing crystalline resistance and easily doped by the sputtering. We observed phase transition characteristics and electrical properties of nitrogen-doped GeSb thin films.

Experiment

We deposited 100 nm thickness of GeSb thin films on glass (soda-lime glass), Si (100)/SiO_2 and Si (100) substrate using a GeSb (99.99%) composite target by a DC magnetron reactive sputtering system at a room temperature. The composition of film varies with deposition conditions, but

S. Y. Lee · H. K. Kim · D. J. Choi (✉)
Department of Ceramic Engineering, Yonsei University, 134 Shinchon-dong, Sudaemun-ku, Seoul 120-749, Korea
e-mail: drchoidj@yonsei.ac.kr

J. H. Kim · J. S. Roh
Memory R&D Division, Hynix Semiconductor Inc., San 136-1, Amiri, Bubal-eup, Ichon-si, Kyoungki-do 467-701, Korea

follows the target composition as is [4]. The composition of the sputtering target we used was 50:50 (Ge:Sb) in atomic %, and therefore we refer to the thin films used in this study as "GeSb thin films." The base pressure was 2.0×10^{-6} Torr and working pressure was 22×10^{-3} Torr which was the most stable plasma condition of our equipment. In order to deposit N-doped GS thin films, nitrogen gas has been introduced during argon sputtering. Total gas flow rate was fixed at 40 sccm and the ratio of argon (99.999%) and nitrogen (99.9999%) gas flow rate has been changed. The nitrogen gas flow rate was changed from 0 to 6 sccm to control the nitrogen concentration of N-doped GS thin films and these are designated as GS(0) and GS(6), respectively. The N-doped GS thin films were annealed at various temperatures from 260 to 450 °C for 20 min by RTA (MILA-3000, UVLAC-RICO, Japan). The relative nitrogen contents were analyzed by secondary ion mass spectroscopy (SIMS, CAMECA IMS-6F) performed with a Cs^+ primary ion source. Sheet resistance of the N-doped GeSb thin films was measured by 4 point probe (CMT-SR2000N, Korea). In order to investigate crystal structure and sub-microstructure of the alloy we analyzed X-ray diffraction (XRD, D/MAX-2500H, Rigaku, Japan) using Cu Kα ($\lambda = 0.15405$ nm) and Transmission Electron Microscopy (TEM, JEM-3010UHR, JEOL) using 0.00197 nm of electron wavelength. Moreover, we observed crystallization speed of N-doped GS thin films by laser irradiation using a static tester (Nanostorage Co. Ltd, Korea) and reflectivity of the films was measured in the range of 400 to 800 nm of optical laser wavelength by UV–VIS spectrophotometer (V-570, JASCO, Japan).

Results

Figure 1 showed the secondary ion intensity of nitrogen in N-doped GS thin films with various nitrogen gas flow rate. The sputtering time was from 20 to 400 s. We found that the relative nitrogen contents increased sequentially as nitrogen gas flow rate increased from 0 to 6 sccm [5]. In addition, the un-doped, where the GS(0), had even some amount of nitrogen, although the intensity was much lower than N-doped GS thin films. This was thought to be because of remnant nitrogen gas in our sputtering chamber or nitrogen gas in the high purity argon gas (99.999%).

We confirmed the nitrogen doping effect on phase transition temperature and structure of N-doped GS thin films by XRD analysis with various temperatures. Figure 2a and b showed N-doped GS thin films XRD results annealed at 400 and 440 °C. All as-deposited films were amorphous. When the annealing temperature was 400 °C, the GS(0) and GS(2) clearly showed Sb hexagonal structure [6], whereas GS(4) and GS(6) showed mixture of amorphous and crystalline state. This was thought to be the

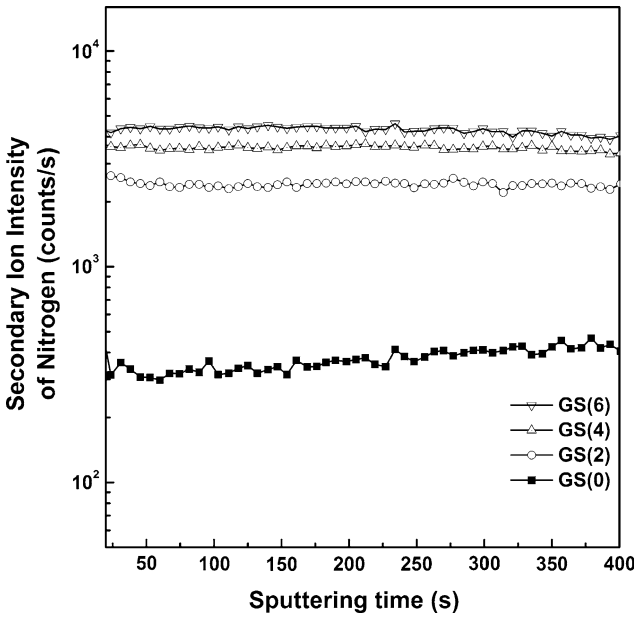

Fig. 1 The secondary ion intensity of nitrogen in N-doped GS thin films

nitrogen reacted with Ge forming nitride during the sputtering and this nitride inhibited phase transition and grain growth during the annealing process [7, 8]. All films showed a crystalline phase at 440 °C, but the peak intensities of N-doped GS thin films were smaller than GS(0). We could understand that the nitrogen doping increases the crystallization temperature of N-doped GS thin films by these results. Moreover, Ge crystal peak appeared in all thin film annealed at 400 and 440 °C. Since Ge and Sb does not have a compound and the solid solubility of Ge in Sb is 2.5 at.% at 520 °C [9], the excess Ge possibly became crystal during the annealing [6, 10]. Therefore, the GeSb film probably had a mixture of Ge crystal and a GeSb solid solution at the temperatures. Figure 3 showed a calculated grain size of N-doped GS thin film annealed at 440 °C. The grain size was calculated based on the full-width at half maximum (FWHM) of Sb (012) using the Scherrer equation:

$$D_{hkl} = \frac{0.9\lambda}{\beta \cos\theta} \quad (1)$$

where D_{hkl} is the grain size, λ is wavelength of Cu Kα ($\lambda = 0.15405$ nm), β is the FWHM value in radian, and θ is diffraction angle. The grain size decreased as nitrogen gas flow rate increased due to nitrogen doping effect, so the electron scattering at the grain boundary happened more often [11].

In order to observe the sheet resistance dependence of various nitrogen gas flow rate and annealing temperature, we measured the sheet resistance of N-doped GS thin films and depicted at Fig. 4. The sheet resistances of all as-deposited

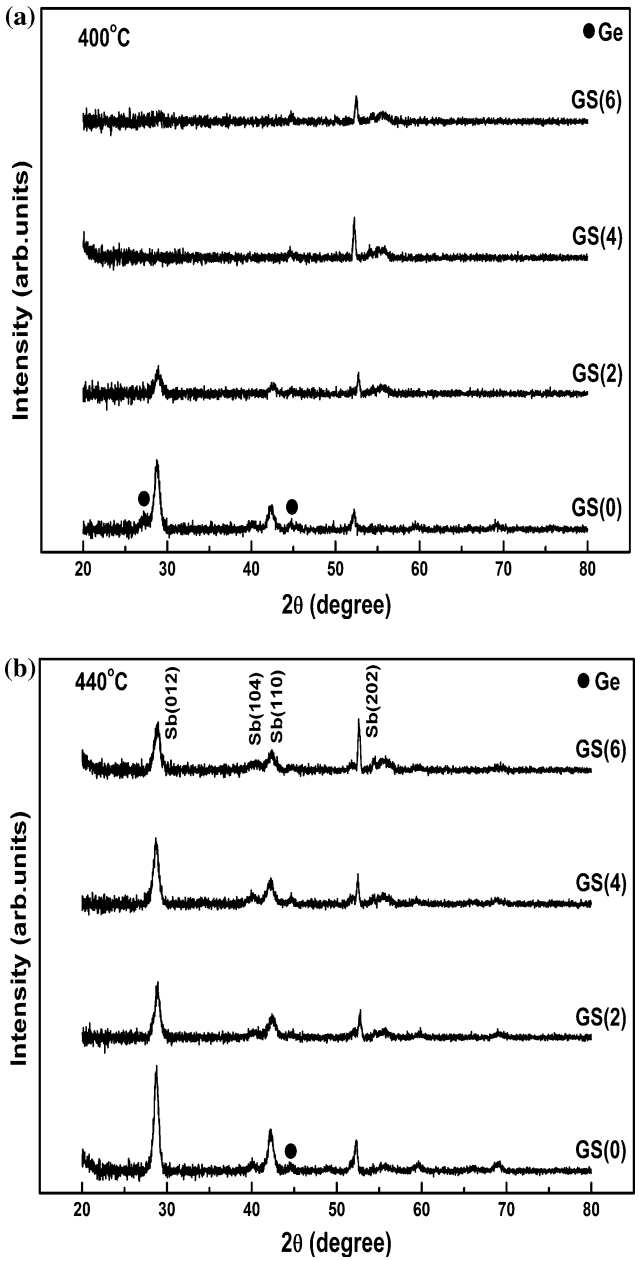

Fig. 2 The XRD analysis of GS(0), GS(2), GS(4), and GS(6) after annealing at **a** 400 °C and **b** 440 °C

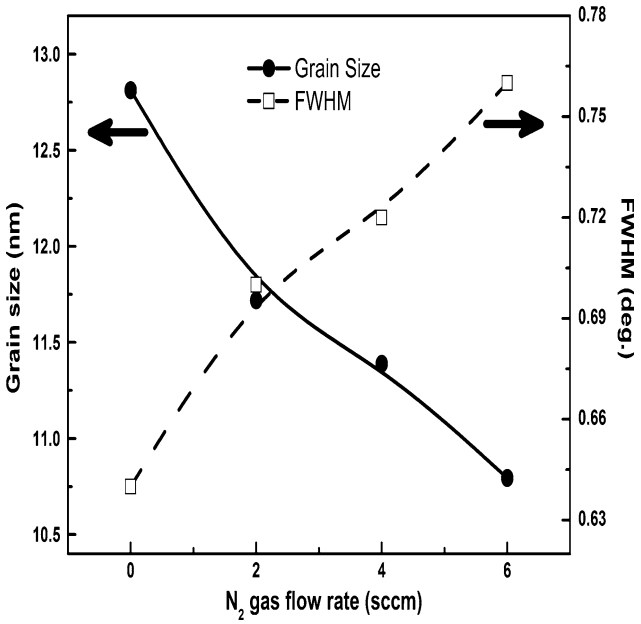

Fig. 3 The FWHM of Sb(012) peak and the calculated grain size with changing nitrogen gas flow rate

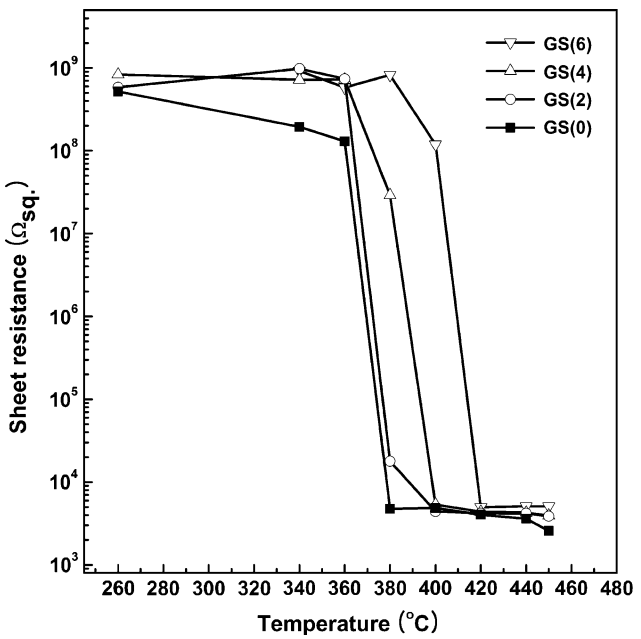

Fig. 4 The Sheet resistance of GS(0), GS(2), GS(4), and GS(6) with various annealing temperature

films were over 10^{12} Ω/□, so we were not able to measure by our analysis equipment due to its over-limit. When the annealing temperature was 450 °C, the sheet resistance of GS(0) was 2.6 kΩ/□, but GS(6) was 5.1 kΩ/□. We found that as nitrogen gas flow rate increased, the temperature, where rapid sheet resistance drop occurs, and crystalline resistance increased. These results were well-matched with the XRD results such as increasing phase transition temperature and decreasing grain size of N-doped GS thin films. These phenomena were easily found in nitrogen-doped chalcogenides, such as N-doped GeSbTe and Sb_2Te_3, called nitrogen doping effect [5, 11].

To further understand the nitrogen doping effect on the sub-microstructure of GeSb thin films, TEM analysis was carried out. Figure 5 depicted the plan view TEM images of (a) GS(0) and (b) GS(6) thin films annealed at 400 °C. The average grain size of GS(0) and GS(6) was 9.7 nm and 6.6 nm which clearly indicated the nitrogen doping suppressed grain growth of GS thin film growth. Moreover, the GS(0) showed polycrystalline of hexagonal diffraction

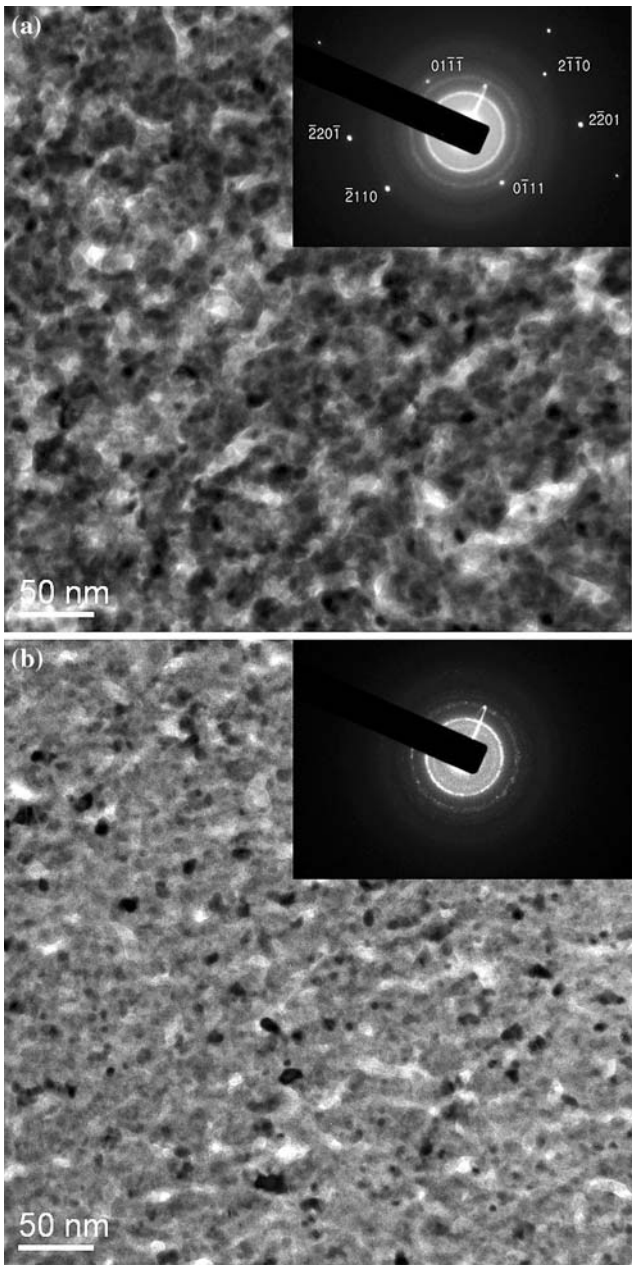

Fig. 5 TEM images and electron diffraction patterns of **a** GS(0) and **b** GS(6) annealed at 400 °C. The GS(0) was polycrystalline of hexagonal structure and zone axis was $[01\bar{1}2]$, whereas GS(6) was mixture of amorphous and crystal

pattern ($[01\bar{1}2]$ zone axis, Fig. 5a), whereas the GS(6) was mixture of amorphous and crystal (Fig. 5b) [6]. These results were well-matched with the XRD and the sheet resistance results. The grain size reduction increased grain boundary scattering so the sheet resistance of GS(6) was higher than the GS(0). In addition, since the GS(6) observed the mixture of amorphous and crystal, we could understand that GS(6) had a higher crystallization temperature than the GS(0).

The crystallization speed is one of important features in PRAM application for fast set operation. To investigate the phase transition property of N-doped GeSb thin films in the scale of nanoseconds, we used a static tester. The static tester measured reflectivity of before and after laser irradiation on the sample using the wavelength of 650 nm laser while changing irradiated laser power and pulse width. Using this reflectivity, the optical contrast (ΔR) was calculated by a following equation:

$$\Delta R = \frac{R_{\text{after}} - R_{\text{before}}}{R_{\text{before}}} \tag{2}$$

where R_{before} and R_{after} indicated the before and after optical reflectivity, respectively. Figure 6a, b showed the Power-Time Effect (PTE) diagram of GS(0) and GS(6) based on the calculated optical contrast with the varying laser power from 1 to 40 mW and pulse width from 10 to 450 ns [13]. The initial region, where laser power and pulse width were low and short, was no change of optical contrast in Fig. 6. In this region the irradiated energy in the films was not enough to activate phase transition, so the optical contrast was not changed. However, when the laser power and pulse width rose at the dashed line in the figures, the optical contrast started to increase by phase transition of the films [13]. This laser power and pulse width called crystallization threshold laser power and time, respectively. In Fig. 6, we found that the crystallization threshold laser power and time of GS(0) were surprisingly higher than the GS(6). To clearly confirm this result, we plotted a relative crystallization of GS(0) and GS(6) when laser power was fixed at 25 mW (Fig. 7a) and laser pulse width was fixed at 250 ns (Fig. 7b). The relative crystallization was calculated by this equation:

$$f_{\text{relative}} = \frac{\Delta R}{\Delta R_{\text{max}}} \tag{3}$$

where ΔR_{max} was the maximum optical contrast [12]. When the laser power was fixed at 25 mW (Fig. 7a), the crystallization threshold time of GS(6) showed 30 ns and the GS(0) was 100 ns. When the laser pulse width fixed at 150 ns (Fig. 7b), the crystallization threshold laser power of GS(6) showed 10 mW and the GS(0) was 22 mW. Especially, there seems to be unstable crystallization occurs in GS(6) when amorphous to crystal phase transition occurs. This phenomenon can be explained by the nitrogen doping effect, through which doped nitrogen forms nitrides and inhibits crystal growth in amorphous film. The films that undergo inhibited crystallization have more grain boundaries acting as light scattering centers when irradiated by laser beam. This may appear to be an effect of unstable crystallization, but the interface scattering effect is a better explanation. According to the XRD, TEM, and sheet resistance results, we expected that the crystallization

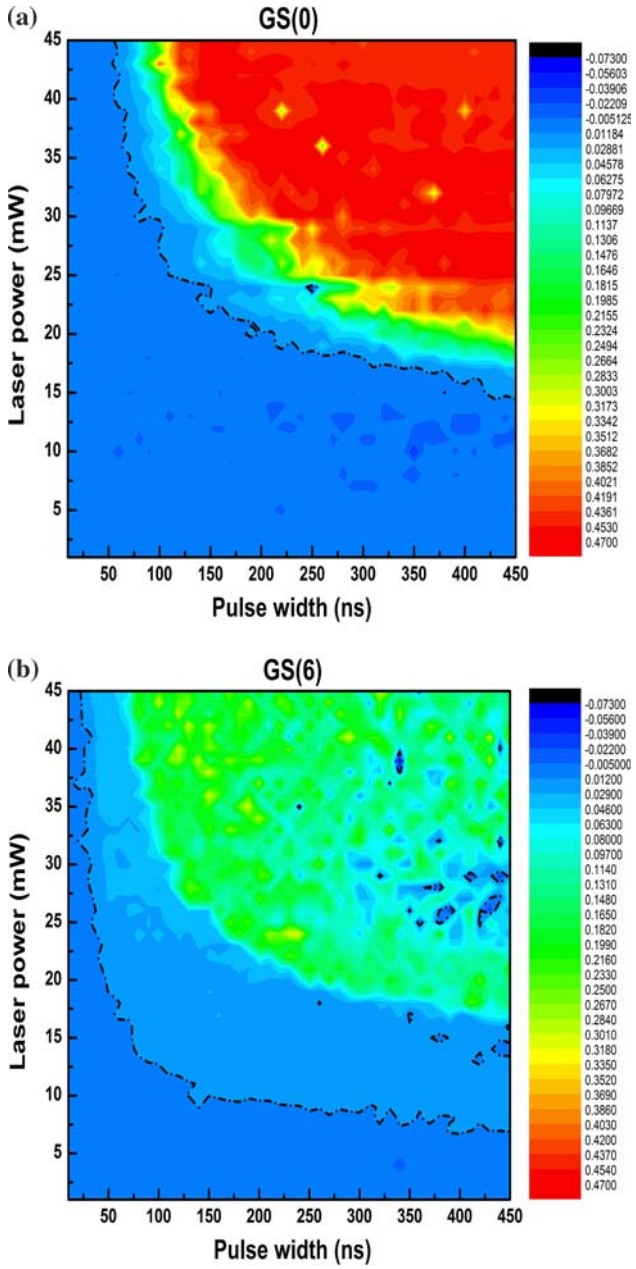

Fig. 6 The PTE diagram of **a** GS(0) and **b** GS(6)

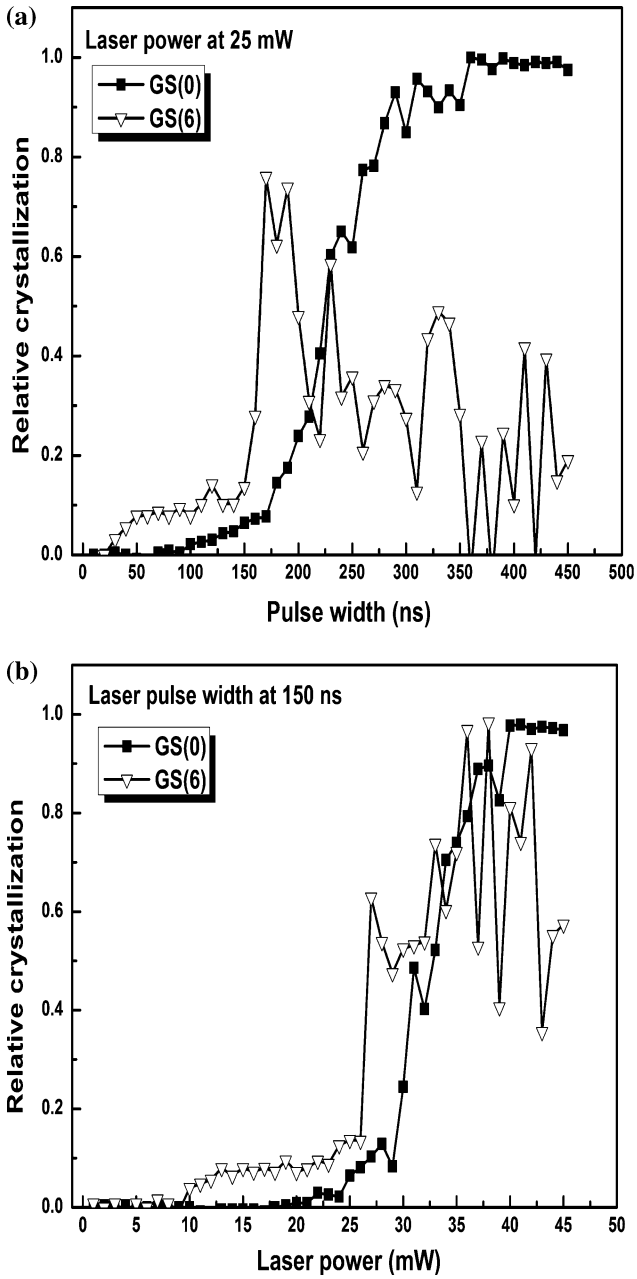

Fig. 7 The relative crystallization of GS(0) and GS(6) fixed at **a** 25 mW laser power and **b** 150 ns pulse width

threshold laser power and time of GS(6) would be higher and longer than the GS(0) due to higher crystallization temperature. However, the static tester results were opposite to our expectation. For finding the reason of this opposite phenomena, we measured the optical reflectivity of GS(0) and GS(6) with changing from 400 nm to 800 nm wave length and showed it in Fig. 8. It was clearly shown that the GS(6) had a lower reflectivity than GS(0) in all wave width, so GS(6) could absorb more optical energy. This is why GS(6) could crystallize at a lower laser power and shorter laser irradiation time than GS(0), even though the crystallization temperature of GS(6) was higher than the GS(0).

Conclusions

The phase transition characteristics and electrical property of the N-doped GS thin films were investigated to understand the nitrogen doping effect on GS using SIMS, XRD, TEM, four point probe, static tester and UV–VIS spectrophotometer in this article. The nitrogen contents of

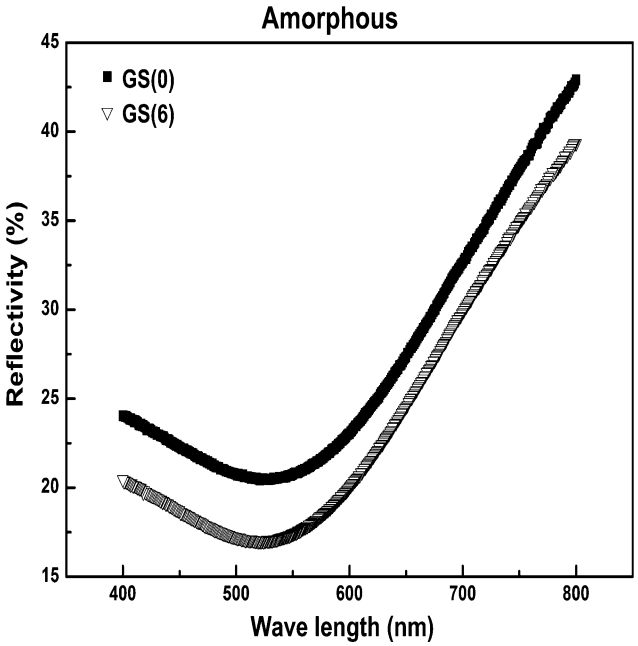

Fig. 8 The optical reflectivity of amorphous GS(0) and GS(6)

N-doped thin films were increased as nitrogen gas flow rate increased. By the XRD and TEM results, as nitrogen gas flow rate increased, the crystallization temperature of N-doped GS thin films was increased which indicated that the nitrogen improve the thermal stability of N-doped GS amorphous state but the grain size was reduced. The sheet resistance of N-doped GS thin films increased from 2.6 to 5.1 kΩ/□ as nitrogen gas increased due to grain size reduction which indicated a possibility of low power reset operation. However, the crystallization threshold time and laser power of GS(0) observed higher and longer than the GS(6) in the static tester analysis due to higher optical reflectivity. Nevertheless, it would be different in PRAM application because PRAM operates by electrical energy. To clearly confirm the nitrogen doping effect on electrical property, we need to have a further analysis by PRAM devices.

Acknowledgements This work was supported by the Second Stage of Brain, Korea 21 project in 2007 and Hynix Semiconductor Inc. of Korea.

References

1. Lankhorst MHR, Ketelaars BWSMM, Wolters RAM (2005) Nat Mater 4(4):347
2. Siegel J, Afonso CN, Solis J (1999) Appl Phys Lett 75(20):3102
3. Chen YC et al (2006) Ultra-thin phase-change bridge memory device using GeSb. In: Electron devices meeting, 2006. IEDM '06 International
4. Ohring M (2002) Material science of thin films, 2nd edn. Academic Press, USA
5. Kim MS et al (2008) Ceram Int 34(4):1043
6. del Pozo JM, Herrero MP, Diaz L (1995) J Non-Crystalline Solids 185(1–2):183
7. Kojima R et al (1998) Jpn J Appl Phys, Part 1 37(4 Suppl B):2098
8. Shin MJ et al (2005) J Mater Sci 40(6):1543. doi:10.1007/s10853-005-0600-4
9. Giessen BC, Borromee-Gautier C (1972) J Solid State Chem 4(3):447
10. Yoo YG et al (2007) Mater Sci Eng A 449:627
11. Horii H et al (2003) A novel cell technology using N-doped GeSbTe films for phase change RAM. In: Digest of technical papers—symposium on VLSI technology, Kyoto
12. Park TJ et al (2008) Curr Appl Phys 8(6):716
13. Kim D-H et al (2005) J Appl Phys 97(8):083535